

Research Article

Anti-Impact Performance Enhancement of Two-Way Spanning Slab through the Implementation of Steel Trussed Bars

Rayeh Nasr Al-Dala'ien ^{1,2}, S. M. Anas ³, and Abdel-Fattah Jamal Kodrg⁴

¹Civil Engineering Department, College of Engineering, Al-Balqa Applied University (BAU), Salt 19117, Jordan

²College of Graduate Studies, Universiti Tenaga Nasional, Jalan IKRAM—UNITEN, Kajang 43000, Selangor, Malaysia

³Department of Civil Engineering, Jamia Millia Islamia (A Central University), New Delhi 110025, India

⁴Custom Engineering Division, ISAT Total Support, La Mirada 90638, CA, USA

Correspondence should be addressed to Rayeh Nasr Al-Dala'ien; rayah.nasr1@bau.edu.jo

Received 23 January 2024; Revised 21 March 2024; Accepted 26 March 2024; Published 12 April 2024

Academic Editor: Vijayanandh Raja

Copyright © 2024 Rayeh Nasr Al-Dala'ien et al. This is an open access article distributed under the Creative Commons Attribution License, which permits unrestricted use, distribution, and reproduction in any medium, provided the original work is properly cited.

Reinforced concrete (RC) slabs represent integral structural components extensively employed in architectural and infrastructural frameworks owing to their inherent robustness and longevity. In contemporary times, there has been a pronounced surge in endeavors aimed at comprehensively elucidating the anti-impact properties inherent in RC slabs. This surge is propelled by a compelling necessity to fortify these structures against the deleterious effects of low-velocity impacts, thereby ensuring their steadfastness and resilience. Consider the thorough investigation into the anti-impact characteristics of RC slabs, which has been rigorously pursued through both experimental and computational methodologies. A plethora of scholarly discourse on this topic is readily available, providing invaluable insights into the structural dynamics governing slabs subjected to low-velocity impacts. However, there is a noticeable gap in research concerning the strengthening of slabs through shear reinforcement, particularly through economical, easily fabricated, and efficient systems such as fabricated trussed bars. The primary objective of this study is to explore the structural behavior of RC slabs fortified with custom-designed trussed bars under the influence of low-velocity impacts. To accomplish this, the Abaqus software platform is explicitly employed for analysis. The slab without any shear reinforcement is experimentally tested and serves as a reference model for numerical verification. Its anti-impact performance is compared with numerical findings. Following validation, simulations are conducted for square slabs strengthened by fabricated trussed bars in orthogonal and diagonal layouts. The results demonstrate that employing fabricated truss bars shear reinforcement with a 3 mm diameter in orthogonal and diagonal layouts enhances the resistance of slabs to damage, resulting in a 28.41% and 47.06% decrease in damage, respectively. The utilization of engineered truss bars as shear reinforcement yields significant improvements in strength, rigidity, and ductility when compared to control samples lacking such reinforcement. This enhancement is particularly evident when the engineered truss bars are arranged in orthogonal and diagonal configurations.

1. Introduction

Impacts, explosions, plummeting objects, or the relentless assault of oceanic surges possess the potential to inflict considerable harm upon concrete edifices, thereby precipitating potentially catastrophic incidents [1]. These occurrences subject structures to a gamut of forces, ranging from abrupt to gradual, or a combination thereof, thereby engendering diverse effects on their constituent elements. Concrete structures, especially those fortified with

reinforcements, confront both localized and extensive deterioration in the face of such exigencies, their manifestation influenced by a confluence of variables such as the magnitude of the force exerted and the inherent vibrational properties of the structure [2]. Pioneering experiments conducted on concrete elements, encompassing beams [3–12], columns [12–14], bridge piers [15], and slabs [16] have provided the foundational framework for comprehending the manner in which structures react to unanticipated and formidable forces [17]. Emphasizing the mechanisms of failure and resistance

inherent to these components, historical studies have often adopted scaled-down replicas for pragmatic purposes, thereby facilitating practical insights into the behavior of concrete structures under duress.

It is crucial to reinforce slabs to prevent disastrous outcomes from sudden, intense forces caused by heavy objects or collisions. Enhancing the strength of slabs involves using stronger materials, additional reinforcement, or specific designs to counter these forces effectively. This not only prevents potential hazards but also improves the structure's durability against such unforeseen impacts, making it a wise investment for both safety and longevity.

Various methodologies and materials have been employed to enhance the durability of slabs under both static and dynamic loading conditions. These include shear studs [18], basalt fiber-reinforced polymer (FRP) strips [19], hybrid fibers comprising hooked-end steel, polypropylene, and Kevlar [20], high-performance fiber-reinforced cementitious composites (HPFRCCs) [21], prestressed concrete [22, 23], ferrocement [24], internal anchorage stirrups [25–27], W-shaped stirrups [28], truss shear reinforcement [29–31], steel plates and slurry-infiltrated mat concrete (SIMCON) laminates [32, 33], polypropylene fiber [33], geogrids [34], and carbon textiles [35]. Increasing the thickness of the slab has demonstrated efficacy in reducing damage and altering failure modes [36], while employing higher-grade concrete has shown some advantages in mitigating slab puncture [37–41].

Employing TRM strips [41] for fortifying concrete slabs against low-velocity impacts can enhance their resilience, diminish surface deterioration, modify the flexural behavior and fracture patterns of the slab, and optimize the absorption and dispersion of energy across the entirety of the structure. Similarly, CFRP can offer improvements in resisting impacts, managing surface damage, and enhancing the structural resilience, with strategic placement and orientation of CFRP strips [42] yielding even better protection. These methods not only offer structural benefits but also provide design flexibility and potential cost savings, especially in retrofitting projects or new constructions aimed at better impact resistance [43–45].

Ultrahigh-performance fiber-reinforced concrete (UHPFRC) stands out due to its superior mechanical properties, promising significant improvements in impact resilience, reduced surface wear, and better managed shape changes during slow-speed impacts. A [45] research effort focuses on identifying the optimal mixtures or fiber ratios in UHPFRC to maximize its dynamic efficiency. This research is crucial for advancing structural design techniques for buildings exposed to slow-speed impacts, potentially broadening UHPFRC's utility in various contexts.

The research endeavors to examine and juxtapose the structural reactions of conventional normal strength concrete (NSC), ultrahigh-performance concrete (UHPC), and steel fiber-reinforced ultrahigh-performance concrete (SFR-UHPC) [46] across varying stress scenarios. Using computational models to mimic the concrete types' behavior, the study examines aspects such as strength, shape alteration, crack development, and modes of failure. The documented improvements in both the robustness and durability of

SFR-UHPC and UHPC align with prior research, presumably attributable to the incorporation of steel fibers. The research approach includes a detailed comparison through computational simulations, essential for guiding design decisions in particular structural settings. Following the implementation of these reinforcement techniques [32–37], there was a noticeable transition in the primary failure mechanism from direct crushing to bending. Additionally, certain strategies have been shown to combine bending with specific localized crushing effects, as noted in earlier investigations [25–27, 29].

The arrangement and direction [47] of bending reinforcement significantly influence the damage patterns in concrete slabs, especially concerning punching or localized damage within the areas of impact. The strategic amalgamation of three tiers of tensioned steel, each positioned with distinct orientations [48], markedly mitigates impact-induced harm, underscoring the pivotal significance of reinforcement alignment in upholding slab integrity. Utilization of diverse dimensions and arrangements of steel bars alongside a welded wire mesh has evidenced that steel structural integrity often deteriorates prior to reaching peak load-bearing capacity. A lack of adequate steel reinforcement can lead to sudden concrete failure, whereas too much reinforcement might cause localized shear fractures.

Research by Hrynyk and Vecchio [49] points out that the rigidity of slabs improves with a higher steel content, suggesting that an increase in reinforcement can bolster slab stiffness and enhance overall structural behavior. This improvement is likely to result in better load management, crack reduction, and structural durability. Similarly, Yilmaz et al.'s [50] research on reinforced slabs underlines the positive impacts of a higher reinforcement ratio, including better bending strength, stiffness, and resilience, alongside reduced deformation.

These observations emphasize the pivotal significance of reinforcement in enhancing the efficacy and durability of slabs when subjected to diverse stressors. Such insights are invaluable for structural engineers, providing practical guidelines for optimizing RC slab designs and construction practices to meet specific project demands. The paramount importance of detailed reinforcement planning cannot be overstated in the pursuit of elevated structural integrity in concrete slabs, providing a cornerstone for the development of more durable and streamlined architectural solutions [17, 39, 40, 51–55].

Stirrups [56] play a pivotal role in bolstering a structure's resilience against impacts through a multifaceted approach, namely, by mitigating cracking, enhancing lateral stability, and augmenting ductility. This allows structures to absorb and distribute the forces from impacts more effectively. Stirrups are essential for preventing cracks, maintaining the structural framework, and ensuring an even distribution of forces across the structure. The careful design of stirrup arrangements, coupled with dynamic evaluations and considerations of material characteristics, is key to achieving the optimal impact resistance in RC structures. Stirrups enhance a structure's defense against dynamic pressures by improving resistance to punching shear and reducing displacements through the strategic increase of shear reinforcement [57].

Shear reinforcement is vital for fortifying slabs against impact forces, boosting their capacity to handle diagonal stresses, and preventing structural failures. Common shear reinforcement elements include stirrups [58], links [57, 59, 60], and shear studs. Stirrups, typically shaped in U or rectangles, are positioned perpendicularly to the principal reinforcement bars to contain and reinforce the concrete against diagonal shear. Internal anchors [25–27, 29–66], situated within the flexural reinforcement's upper and lower bounds, enhance structural integrity. Links, forming closed loops [67], offer similar advantages and are often utilized in columns [12, 13, 68] and beams [69–71]. Shear studs [72], found in composite constructions, ensure an effective shear connection between the steel and concrete components. Inclined shear reinforcements, such as angled stirrups or truss systems [29–31], counter diagonal tension and inhibit crack growth. The choice of shear reinforcement configuration is shaped by factors such as load parameters, structural design considerations, and precise engineering mandates. This underscores the pivotal significance of shear reinforcement in augmenting both the resilience and operational efficacy of RC elements when subjected to dynamic loads.

Trussed bars represent a highly effective means of augmenting shear resistance within slabs, owing to their adeptness in proficiently managing diagonal tensile stresses. The triangular configuration of these bars allows for the effective distribution and redirection of shear forces, thereby enhancing the slab's resilience to such stresses. This geometrically favorable design ensures optimal reinforcement material usage, reducing the need for excess steel while maximizing shear resistance. Trussed bars' adaptability to various slab geometries enhances their utility across a range of structural applications. Additionally, their ease of installation presents a cost-effective reinforcement solution, compliant with industry standards and construction practices. The empirical evidence supporting the use of trussed bars in concrete reinforcement underscores their proven efficacy in enhancing slab shear resistance [29–31].

However, the literature reveals significant research gaps in the application of trussed bars for slab reinforcement. Despite the reliance on computational modeling, there is a marked scarcity of empirical and numerical data, highlighting the imperative for thorough experimental validation. Real-world data are crucial for a reliable assessment of trussed bars' effectiveness and practical utility. Moreover, a detailed exploration of design variables, such as the shape and spacing of truss bars, is necessary to fully understand their impact on performance. The interaction dynamics between the concrete slabs and trussed bars, particularly under impact loading conditions, warrant an exhaustive investigation to uncover their behavior and potential for performance improvement. It is imperative to address these lacunae in research in order to acquire a thorough comprehension of the operational efficacy of trussed bars. Such understanding is pivotal as it serves to elucidate and refine their utilization in bolstering the durability and resilience of RC slabs against the rigors of impact stresses.

2. Experimental Arrangement and Specimen Configuration

In pursuit of conducting rigorous examinations, three RC solid slabs measuring $800 \times 800 \times 90$ mm have been fabricated. Subsequent sections will meticulously scrutinize the testing methodologies employed in this investigation.

2.1. Experimental Samples and Constituents. The slabs were fabricated utilizing 6 mm steel rods as primary and ancillary reinforcement, boasting a yield strength of 560 MPa, adhering rigorously to the guidelines set forth by the ASTM E8/E8M standards. The consistent placement of the steel bars throughout the slab enhances its load-bearing capacity and resistance to bending moments [73].

The slab design described in Figure 1 includes specific dimensions and reinforcement details in accordance with the ACI codes. The combination of two concrete covers, with a thickness of 10 mm at the base and 20 mm at the apex, augmented by an additional 50 mm cover on each side, ensures comprehensive protection for the embedded reinforcement, thereby significantly contributing to the resilience and longevity of the slab. The flexural bars, which are uniformly sized and evenly spaced in both directions, provide reinforcement against bending moments. The steadfast steel proportions, with $\rho = 0.37\%$ allocated for flexural tension reinforcement and $\rho' = 0.37\%$ designated for compression reinforcement, align seamlessly with the design criteria outlined in ACI 421.1R-08 for a solid slab [26, 29, 40, 74–77]. The thickness of the slab adheres to the stipulations delineated in the ACI code 9.5.3, thereby guaranteeing structural robustness and alignment with prescribed design criteria. In its entirety, the design meticulously conforms to the paramount standards of the industry and regulatory mandates, thereby safeguarding the structural robustness and operational efficacy of the slab.

The targeted compressive strength of the slabs was set at 30 MPa, prompting the formulation of a concrete mix ratio tailored to achieve this specification. Three $10 \times 10 \times 10$ cm cube samples were taken from each batch, trowel-straightened, and vibrated to remove air voids. After curing for 28 days, the concrete's compressive strength was determined using axial load testing [78], with results converted to cylindrical strength as per Eurocode-2 (1992-1-1) [79] recommendations. This standardized testing procedure ensures accurate evaluation of concrete strength, providing crucial data for assessing the performance of the RC slabs.

2.2. Instruments and Test Devices. The contemporary investigation employed the drop-weight impact assessment method, initially formulated by ACI Committee 544 in 1988 [80]. Crucially, it is imperative to note that the descent distance remains consistent throughout the experiment, with the apparatus capable of attaining a maximum descent height of 1200 mm. Various weights of different diameters can be released from different drop distances using this setup. The pivotal component of subjecting the test specimens to impact loading is the impactor, also referred to as

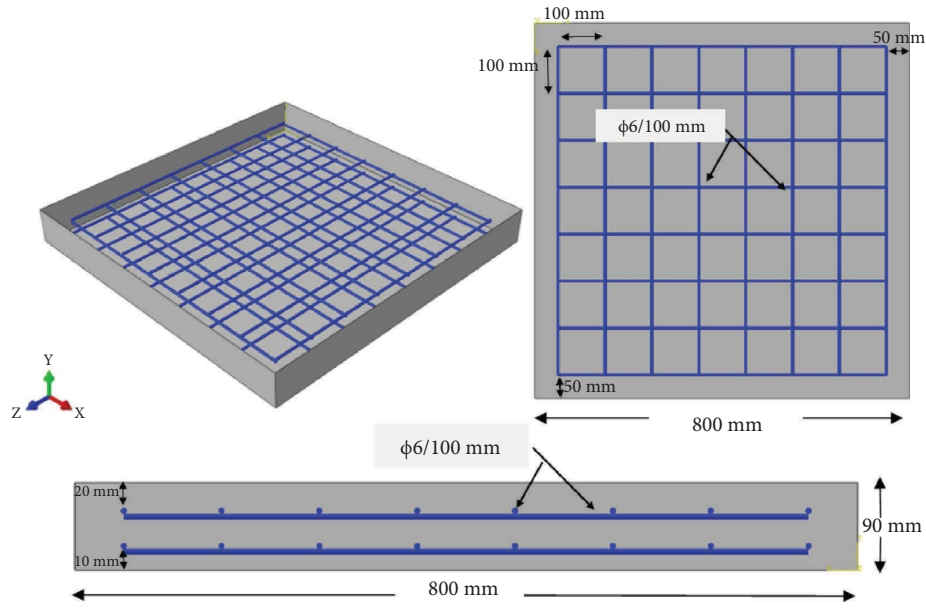


FIGURE 1: Steel configuration for the control sample.

the hammer. Crafted from high-strength steel, it is meticulously engineered to ensure both longevity and uniform dispersion of impact forces. Deliberately, an eccentric load is imposed, with precise coordination, positioning the targeted impact point at coordinates (20, 20) mm away from the central axis of the slab, as depicted in Figure 2.

In the present analysis of impact testing, the magnitude of energy imparted onto the specimens is contingent upon both the mass of the steel hammer and the altitude from which it is released. In order to maintain uniformity, the experiment was structured to administer a homogeneous force of impact totaling 176.58 Joules. This was accomplished by utilizing a hammer mass of 40 kilograms and a drop height of 450 millimeters. Careful consideration was given to the parameters to accurately track specimen degradation. This included accounting for the measurement constraints of the experimental instruments when calculating the impact loading energy.

Within impact assessments, the experimental framework integrates an array of sophisticated measuring apparatuses to procure vital data. The principal instruments utilized within this experimental initiative encompass accelerometers, LVDTs (linear variable differential transformers), dataloggers, steel strain gauges, and concrete strain gauge systems. These instruments are crucial for capturing important parameters such as acceleration, displacement, strain, and other dynamic responses during impact testing. Table 1 furnishes an exhaustive inventory delineating the array of tools incorporated within the experimental configuration, accentuating the breadth of instruments deployed to facilitate meticulous data collection and analysis. Concurrently, real-time data are projected onto the digital interface of the testing apparatus, while a data logger boasting 16 channels adeptly captures the measurements derived from assorted sensors. The amassed dataset

encompasses temporal trajectories of displacement, acceleration, concrete strain, and steel strains.

Under hypothesized supporting conditions, C-channel steel sections securely anchor the specimens on all four sides. Impact testing ceases upon the failure of all specimens, with maximum displacement values meticulously documented. Visual inspections are conducted to assess concrete cracking and the integrity of steel reinforcements. The esteemed software developed by IMC meticulously analyzes the data, unveiling intricate failure mechanisms and structural responses under dynamic loads. The comprehensive testing protocol meticulously evaluates the impact resistance of RC slabs. Figure 3 provides a graphical depiction illustrating the strategic placement of strain gauges affixed to the primary steel during experimental procedures. Table 2 and Figure 4 present the experimental findings obtained from the instrumentation installed in the control samples.

Since control sample 1 had an average total number of drops of 124, as shown in Table 2, the sample results were taken into consideration during the discussion.

The cumulative kinetic energy exerted upon the control specimen, designated as “ N ” (mgh), is computed utilizing the equation wherein “ m ” symbolizes the mass of the hammer, “ g ” denotes the gravitational acceleration, “ h ” signifies the altitude of descent, and “ N ” reflects the count of successive drops.

The cumulative kinetic energy exerted on the control sample amounts to 21895.92 Joules, calculated through the formula: 124 multiplied by 40, then by 9.81, and finally by 0.45.

Upon scrutinizing the empirical findings, it became evident that the control specimens underwent significant structural compromise, characterized by slab perforation and top-face punching failure. Furthermore, sample 3 displayed the manifestations of scabbing and concrete

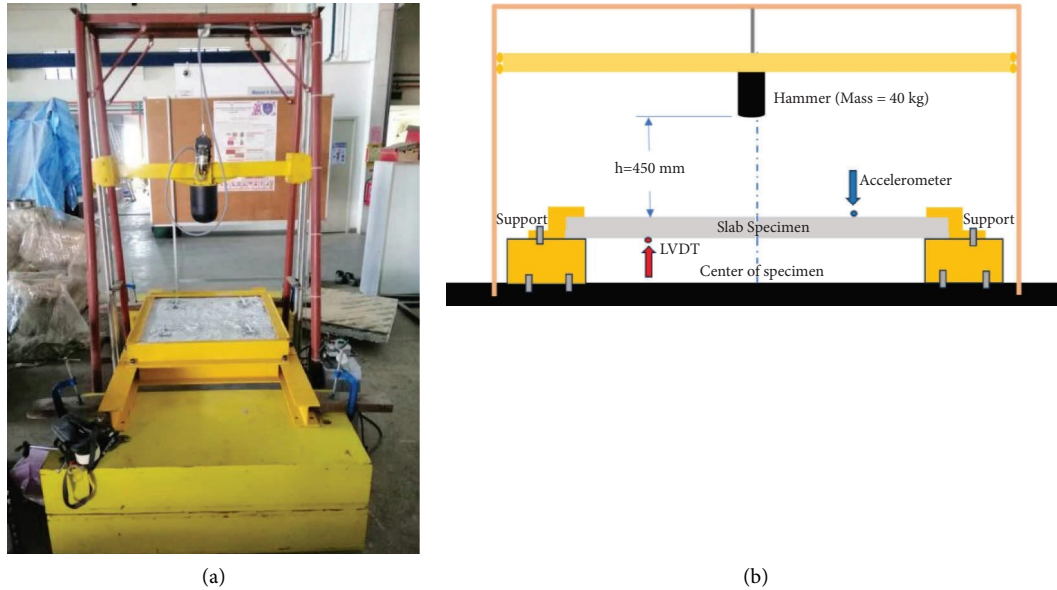


FIGURE 2: Arrangement of the drop-weight impact test configuration. (a) Drop-weight instrument. (b) Schematic drawing of the test setup.

perforation. Furthermore, there were signs of flexural bond deterioration and diagonal and intermittent cracks observed on the lower slab surface, as illustrated in Figure 5.

3. Finite Element Analysis and Verification

In this structural engineering investigation, Abaqus is employed to construct finite element representations of RC slabs. The facile simulation of both dynamic and static loads facilitates intricate numerical scrutiny. Abaqus is favored for its adeptness in exploring intricate phenomena such as high-velocity impacts, contact mechanics intricacies, and deformations in structural components. Its utilization is widespread among engineers and projects owing to its capability in utilizing advanced material models and precise failure criteria, culminating in meticulous and reliable results [81].

Concrete slabs, steel reinforcement, impactors, and C-sections (slab boundary components) are all modeled in three dimensions using Abaqus software in structural engineering. The process of modeling entails the meticulous allocation of suitable material attributes to individual components. This involves the software configuring three discernible material classifications: concrete, steel reinforcement bars crafted from HRB500 steel, and the steel hammer constructed from linear elastic steel [82].

To gain deeper insights into the stress-strain interplay in both compression and tension scenarios, scholars resort to employing the concrete damaged plasticity (CDP) model. This sophisticated model aptly captures the intricate nonlinearities inherent in concrete behavior. Detailed elucidations of the material properties pertaining to concrete and steel are meticulously documented in Tables 3 and 4, respectively.

To elucidate the interrelationship among diverse geometries, a comprehensive contact interaction, as delineated

in reference [83], is employed. This interaction encompasses both tangential and rigid contact behaviors and assumes a friction coefficient of 0.02 at the contact interface, as referenced in Ref. [42]. Furthermore, the integration of an embedded region constraint fortifies the linkage between the encompassing concrete substrate and the steel reinforcements, thereby augmenting structural robustness and load-bearing capacity, as articulated in Ref. [84]. Concerning boundary conditions, the edges of the slab are wholly fixed to emulate the experimental configuration. Steel C-sections are instantiated on each periphery of the slab to emulate rigid support, as elucidated in Ref. [84], mirroring the experimental test conditions and precluding any potential motion or deformation. To mitigate energy dissipation due to steel deformation under stress, the design of the steel hammer incorporates a rigid body. Two distinct sets of boundary conditions are applied: specialized constraints for the hammer, confining its motion solely to the vertical (y) axis, and fully fixed (ENCASTRE) conditions for the supporting framework, as referenced in Ref. [81].

The numerical framework has been meticulously crafted to integrate the implementation of recurrent low-velocity impact loading, aligning precisely with the experimental test configuration. A predetermined height above the upper surface of the slab is designated for the hammer's elevation, following which it is released, descending freely under the influence of gravitational force. This descent occurs singularly, characterized by a distinct velocity. The determination of the free-fall velocity and the duration of the descent is achieved by employing established equations that faithfully capture the specific conditions intrinsic to the experimental setup. The scrupulous application of numerical methodologies guarantees a precise depiction of the dynamic responses exhibited by RC slabs under the influence of impact load,

TABLE 1: Instruments of the experimental part.

Measure	Device	Location
Acceleration	Piezoelectric accelerometer KS77C.10 ± 600 g	At a distance of 200 mm from the centroid of the experimental specimen
Vertical displacement	LVDT	Position 200 mm from the midpoint of the underside of the slab
Strain in steel	KYOWA brand steel strain gauge	Within the sample, two steel bars are situated, with one positioned at the uppermost section and the other at the lowermost, maintaining a separation distance of 200 mm from the sample's center
Strain in concrete	KYOWA brand concrete strain gauge	The offset from the central axis of the underside of the specimen's hammer measures 200 mm

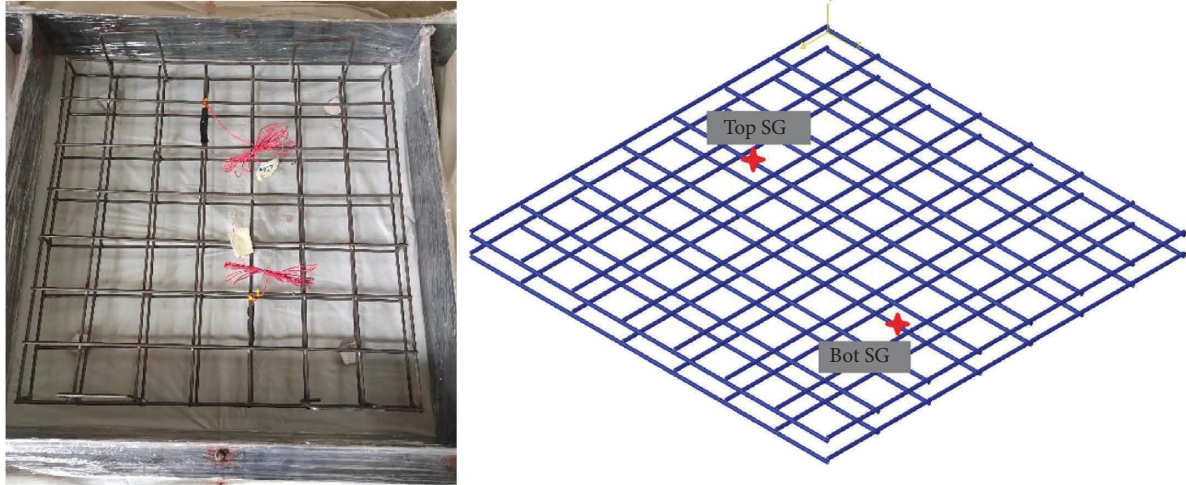


FIGURE 3: Steel strain gauges mounted on the main reinforcement.

$$\begin{aligned}
 v_{\text{free-fall}} &= \sqrt{2gh}, \\
 &= 2.97 \frac{\text{m}}{\text{sec}}, \\
 t_{\text{free-fall}} &= \sqrt{\frac{2h}{g}}, \\
 &= 0.30289 \text{ sec}, \\
 &= 302.89 \text{ ms}.
 \end{aligned} \tag{1}$$

Within this framework, symbol “ g ” symbolizes the gravitational acceleration (9.81 mm/s^2), while “ h ” denotes the descent height (450 mm).

Upon finalizing the generation of finite element models, each component underwent a meticulous meshing process, whereby it was subdivided into smaller constituents. Meshing stands as a critical operation necessitating iterative exploration to ascertain the optimal mesh size that strikes a balance between precision and computational efficiency. The duration of computational processes is significantly influenced by the mesh size, thereby rendering it a pivotal factor for consideration. Table 5 elucidates the node and element counts for the specimens. Figure 6 offers a comparative depiction of acceleration-time history plots for various mesh sizes of RC slabs during the initial impact of the drop weight. The investigation concludes that a 10 mm element size closely corresponds with the experimental observations. Furthermore, Figure 6 illustrates the formation of the finite element model subsequent to the meshing process.

The process involved reviewing various finite element models and conducting dynamic explicit nonlinear analysis. This method allowed for the comparison of numerical data with experimental results obtained through measurements.

The calibration procedure stood as a pivotal endeavor, indispensable in guaranteeing the precision and

dependability of the numerical model. This intricate process entailed the iterative refinement of both model parameters and input variables, meticulously constrained within permissible margins, to harmonize the numerical outputs closely with empirical observations. The paramount objective remained the cultivation of a robust numerical model, one distinguished by its faithful depiction of the slabs’ response to impinging forces.

Following the calibration process, a thorough juxtaposition of numerical results against experimental data was undertaken, with meticulous scrutiny of pivotal performance metrics and influential factors delineated in both Tables 6 and 7. This meticulous comparative analysis served to illuminate the veracity and precision of the numerical model employed (Figure 7). Furthermore, Figure 8 presents the acceleration-time profile observed during the inaugural descent, furnishing visual elucidation on the manner in which the slabs reacted to the impinging force. This graphical representation facilitated the comprehension of the alterations in velocity experienced by the slabs throughout the duration. Moreover, Figure 9 juxtaposed the authentic failure mode against the finite element model’s failure mode across specimens featuring varied scabbing concrete widths, thereby furnishing a graphical elucidation of the concordance between empirical and computational outcomes.

Tables 6 and 7 stand as exhaustive validation tools for the finite element model, showcasing its precision in prognosticating acceleration magnitudes during the onset of descent. This validation extends to the control specimen, with the model exhibiting an accuracy of 1.8% for the control sample when compared to the experimental results. The finite element model accurately predicts steel strain at failure, within an 8% margin compared to experimental data. Figure 8 shows similar peak acceleration and duration, indicating agreement between the experiments and simulations under impact loads. The model effectively captures slab behavior, bolstering confidence in its accuracy and numerical analysis results.

Moreover, in accordance with the failure mode illustrated in Figure 9, a notable concurrence emerges in the manner of failure, encompassing concrete scabs, diagonal

TABLE 2: Experimental results from installed instruments of control samples.

Specimen	Acceleration (g)		Complete failure		The mean number of drops until initial cracking	The mean drop count until total deterioration	Initial deformation of concrete upon impact ($\mu\epsilon$)		Primary steel strain at initial impact ($\mu\epsilon$)		Reduction in primary steel strain upon complete failure ($\mu\epsilon$)	
	First drop Max	First drop Min	Max	Min			Left	Right	Top	Bottom	Top	Bottom
Control sample 1	90.38	-79.87	197.4576	-290.4			185	226.9	155.88	337.2	188.34	535.98
Control sample 2	102.5	-98.7	180.9	-224.96	5	124	177.5	301	213	378	254.852	656.2
Control sample 3	92.78	-104.67	191.64	-298.79			248.7	347.66	171	259	144.866	499.2

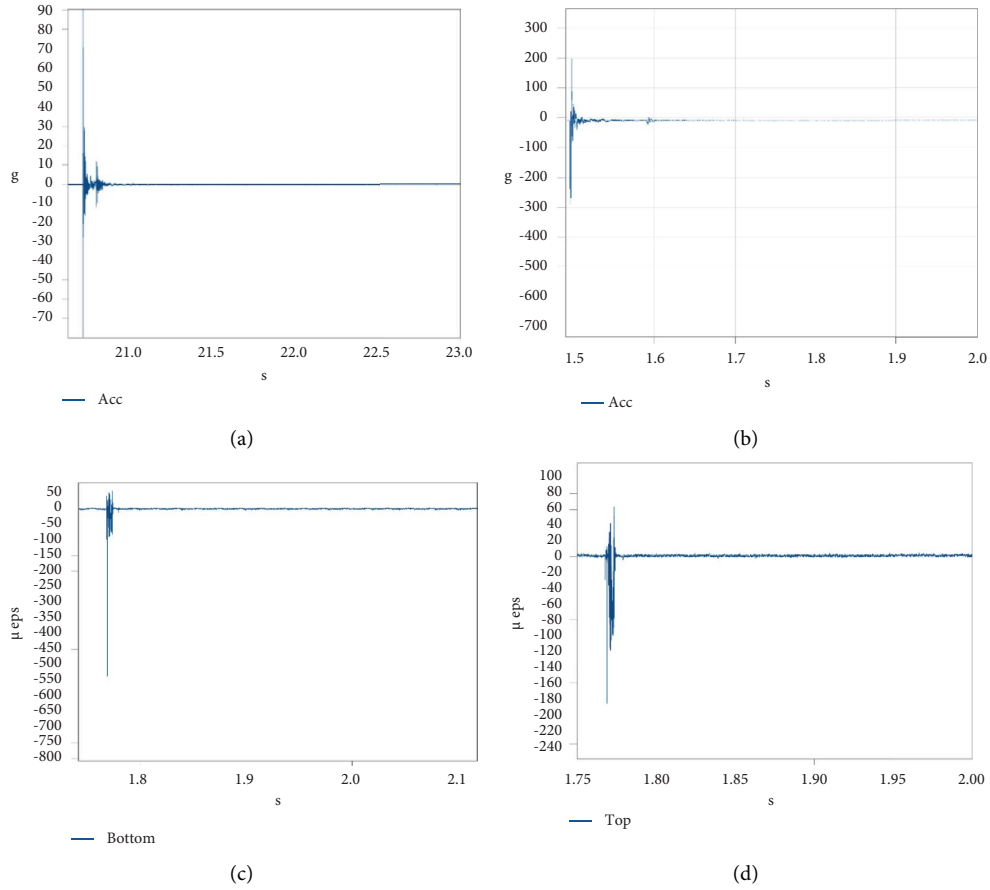


FIGURE 4: Findings from the control specimen acquired via instrumentation deployed within the experimental configuration. (a) Acceleration-time profile during the initial drop. (b) Acceleration-time profile upon total failure. (c) Temporal evolution of strain in bottom primary steel. (d) Temporal evolution of strain in primary top steel.



FIGURE 5: Control samples' failure modes.

TABLE 3: Characteristics of concrete and (CDP) parameters.

Property	Value
Poisson's ratio	0.2
Density (kg/m^3)	2351
Modulus of elasticity (MPa)	27325
Compressive strength (F_C) (MPa)	33.7
ψ	30
E	0.1
σ_{bo}/σ_{co}	1.166
K_C	0.66667
μ	0.0001

TABLE 4: Characteristics of steel material.

Property	Steel rebars	Steel hammer
Poisson's ratio	0.3	0.3
Density (kg/m ³)	7851	7850
Modulus of elasticity (MPa)	200 × 10 ³	200 × 10 ³
Yield stress (MPa)	568.488	568.48
Ultimate stress (MPa)	603.391	—

TABLE 5: Quantity of nodes and elements.

Specimen	Node count	Element count
Control	69247	60796
Trussed bar control model	69945	61408

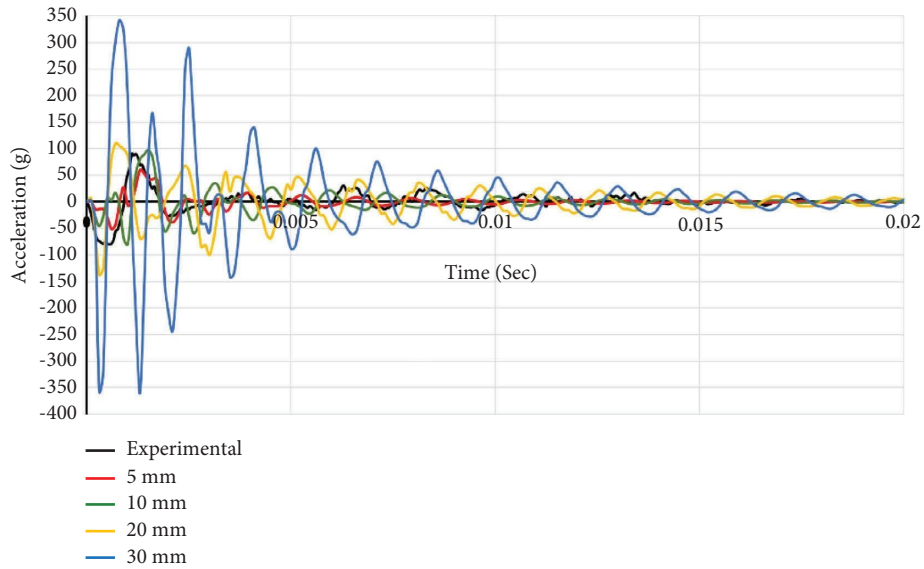


FIGURE 6: Comparing acceleration-time profiles of control sample RC slabs with varying element sizes upon initial drop weight impact.

TABLE 6: Comparison of acceleration values.

Specimen No	Initial drop acceleration (g)				Ratio ⁺	
	Practical investigation		Computational analysis		%	
	Max	Min	Max	Min	Max	Min
Control	90.38	-79.87	88.76	-80.03	1.8	0.2

⁺Ratio = |(Experimental value minus numerical value) divided by experimental value|%.

TABLE 7: Comparison of strain values for steel at full failure: experimental and numerical analyses.

Sample	Strain (με)				Ratio ⁺	
	Computational analysis		Practical investigation		%	
	Top	Bot	Top	Bot	Top	Bot
Control	75.041	222.861	69.991	219	7.22	1.76

⁺Ratio = |(Experimental value minus numerical value) divided by Experimental value|%.

cracks, and the lack of bending between steel and the enveloping concrete, between the experimental and FEM findings. Additionally, the extent of scabbing concrete

exhibits a striking resemblance between the experimental and FEM results, differing by a mere 4% in comparison with the experimental outcomes.

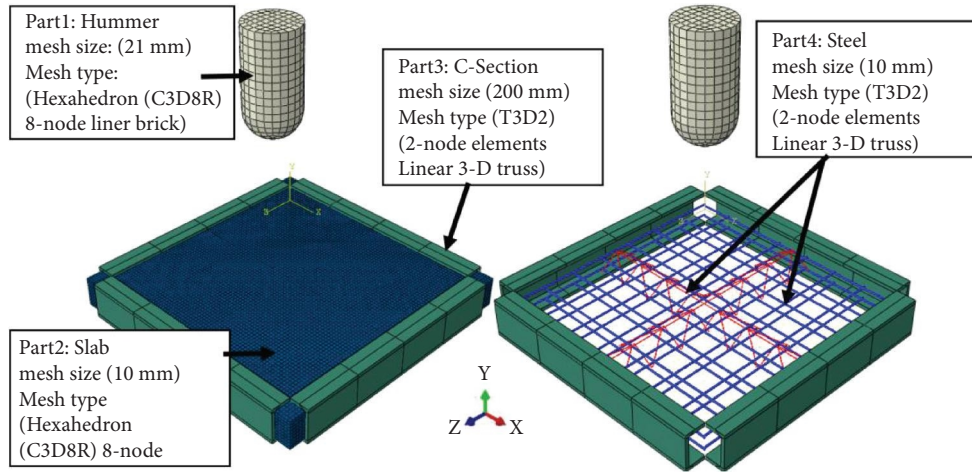


FIGURE 7: Finite element model details.

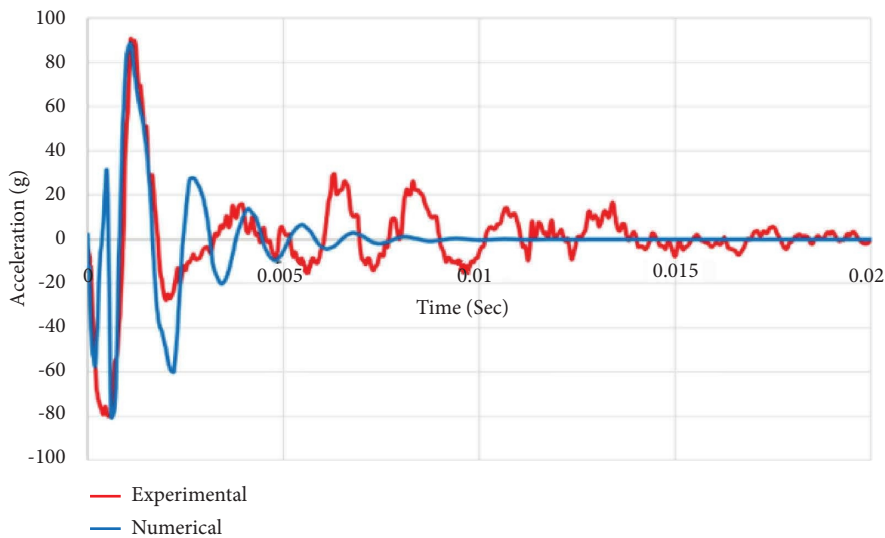


FIGURE 8: Comparing acceleration-time profiles in the initial drop phase: experimental versus numerical results for the control sample.

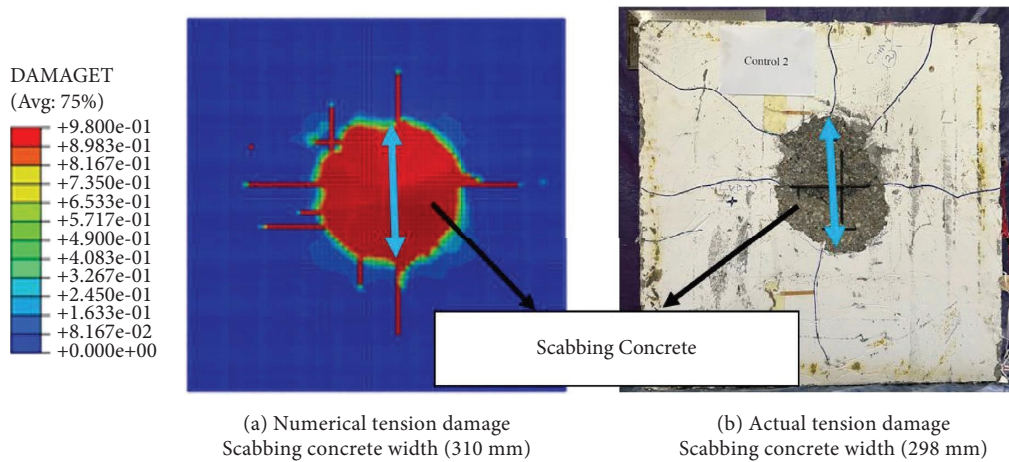


FIGURE 9: Comparative analysis of failure mechanisms in control sample total failure: experimental vs. numerical data.

The test findings from the practical examination closely paralleled the envisaged failure modalities, particularly emphasizing phenomena such as punching shear and the disintegration of the bond between steel and concrete. Mesh size limitations led to discrepancies, especially in truss bar samples' inability to clearly show fractures. Differences between numerical predictions and real-world outcomes were attributed to concrete's nonhomogeneous nature [85] and varying support conditions, not adequately captured by models assuming homogeneity. These variations arise from factors such as compaction and curing conditions, altering material characteristics.

Additionally, numerical analyses, though precise in addressing support conditions, might disregard pragmatic factors such as friction or displacement among supports under impact loading. The omission of strain rate effects could similarly account for variations noted in dynamically stressed concrete. The existing CDP [86] material model did not fully consider concrete's strain rate dependence, especially under dynamic loading. The authors proposed enhancing the CDP model by integrating stress-strain characteristics dependent on the strain rate, thereby offering a more adept approach toward mitigating dynamic impacts [87].

4. Parametric Study

After the proficient validation of the finite element simulation, a parametric investigation was initiated to delve into the dynamic characteristics of RC slabs fortified with truss bars for shear reinforcement when subjected to low-velocity impact loads. This investigation sought to evaluate the influence of various parameters on the behavior of slabs, incorporating factors that may pose challenges for experimental assessment due to constraints related to time, labor, and expenses. Figures 10 and 11 delineate the structural layout parameter pertaining to the fabricated trussed bar shear reinforcement examined in this study. Despite subjecting all specimens to an identical number of loading cycles (124 drops), the parametric analysis involving slabs reinforced with trussed bar shear reinforcement enabled an exploration of the effects of this reinforcement technique and its layout parameters on structural response under controlled experimental conditions. To enhance clarity in discussing the specimens, a system of naming conventions is detailed in Table 8, while Figure 12 provides the visual representations of the finite element models employed for the parametric study specimens.

Flexural tension and compression reinforcement were assessed, yielding steel ratios of $\rho = 0.37\%$ and $\rho' = 0.37\%$, respectively. Equation (2) was employed to calculate the transverse steel ratio, encompassing the vertical legs of the truss bars, for both inclined and vertical truss bars shear reinforcement,

$$\rho_{t\phi} = \frac{2A_{st}}{bs \sin \phi_1} + \frac{2A_{st}}{bs \sin \phi_2}. \quad (2)$$

In the above equation, A_{st} represents the area of the shear reinforcement in the form of truss bars with two legs linked

together. These truss bars are 3 mm in diameter. The variable "s" symbolizes the consistent interval between shear reinforcement elements. Furthermore, ϕ_1 and ϕ_2 denote the angles formed between the forefront of the truss bar reinforcement and the vertical link, as well as their alignment with the truss bar reinforcement and the axis perpendicular to the exerted shear force, respectively.

The slab adheres meticulously to the parameters delineated within the ACI code 9.5.3 concerning thickness, while the steel ratio impeccably aligns with the design constraints as articulated in ACI 421.1R-08 for RC solid slabs.

Adhering to the directives delineated in ACI 318-19 and ACI 421.1R-08, it is imperative to employ the method of uniformly distributing shear reinforcement around the pivotal section's centroid. This approach is crucial to guaranteeing the convergence of the failure surface of the slab with the peripheries of the shear reinforcement, thereby augmenting the structural efficacy and load-bearing capacity of the edifice.

Ensuring the symmetrical placement of shear reinforcement, as depicted in Figures 10 and 11, is imperative for achieving uniform distribution of loads and forces throughout the slab. This practice fosters a well-calibrated system for transferring loads and mitigates the likelihood of localized structural failures. Notably, shear stresses tend to amplify at critical junctures, underscoring the significance of this methodology. Comprehensive analyses detailing failure modes for each variation within the parametric study are exhaustively outlined in Table 7. Furthermore, numerical findings pertaining to the study samples are comprehensively documented in Tables 8 and 9. Visual representations elucidating the numerical outcomes are vividly illustrated in Figures 12–14.

5. Results and Discussions

The findings from the experimental, numerical, and parametric research studies conducted in this study are thoroughly covered in the following subsections.

5.1. Damage Profile. As per the findings delineated in Table 9, the degradation extends diagonally toward the peripheries of the slab, albeit manifesting in a less pronounced manifestation of the flexural mode. Concrete serves to alleviate damage in the flexural mode by circumventing diagonal fractures. The pristine slab (designated as C ϕ 6*) demonstrates a cumulative damage due to energy (DDE) amounting to 77.205 J at the 124th drop, whereas the specimens incorporating engineered truss bars (denoted as TB ϕ 3Orth and TB ϕ 3Dia) register cumulative DDEs of 55.2723 J and 40.8717 J, respectively, at an equivalent number of drops.

The study endeavors to ascertain whether the incorporation of shear reinforcement in orthogonal directions could mitigate the vulnerability of the slab to punching failure. The inclusion of shear reinforcement demonstrates a marked reduction in punching, flexural bond failure, and

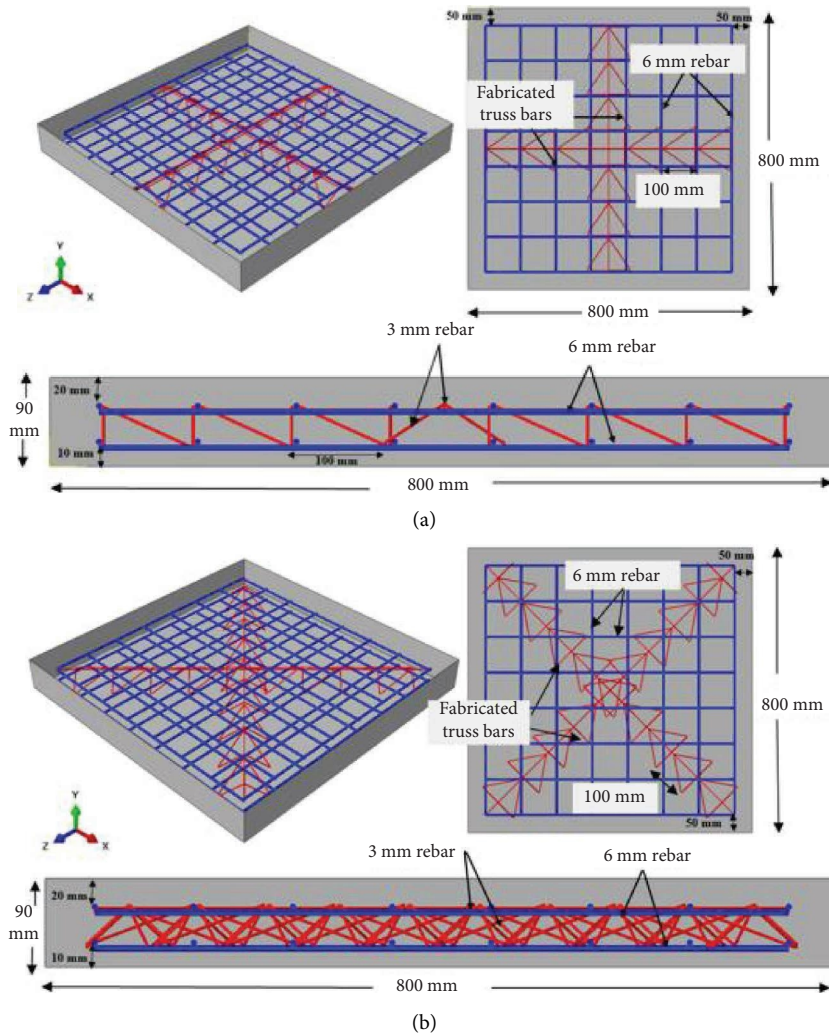


FIGURE 10: Steel mesh details of samples with fabricated truss bar. (a) Sample with fabricated truss bar in orthogonal orientation (TBφ3Orth). (b) Sample with the fabricated truss bar in diagonal orientation (TBφ3Diag).

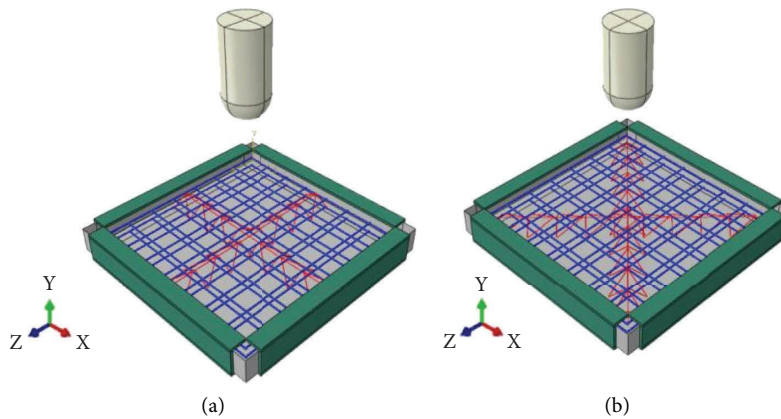


FIGURE 11: Finite element model of samples with fabricated truss bars. (a) Sample with the fabricated truss bar in orthogonal orientation (TBφ3Orth). (b) Sample with the fabricated truss bar in diagonal orientation (TBφ3Dia).

the emergence of diagonal fractures at the underside in contrast to control specimens devoid of such reinforcement. The extent of damage suffered by a slab reinforced with shear

is notably inferior to that experienced by the reference control slab upon complete failure, showcasing a reduction of 28.41% (TBφ3Orth*) and 47.06% (TBφ3Dia*) relative to (Cφ6*).

TABLE 8: Names of samples for parametric study.

Sample	Parameter	Bar diameter	Name	Shear reinforcement steel ratio
With truss bars	Arrangement	$\phi 3$	TB $\phi 3$ Orth	0.003482234
		$\phi 3$	TB $\phi 3$ Diag	0.003482234

ϕ : bar diameter; Orth: orthogonal; Diag: diagonal; TB: truss bars.

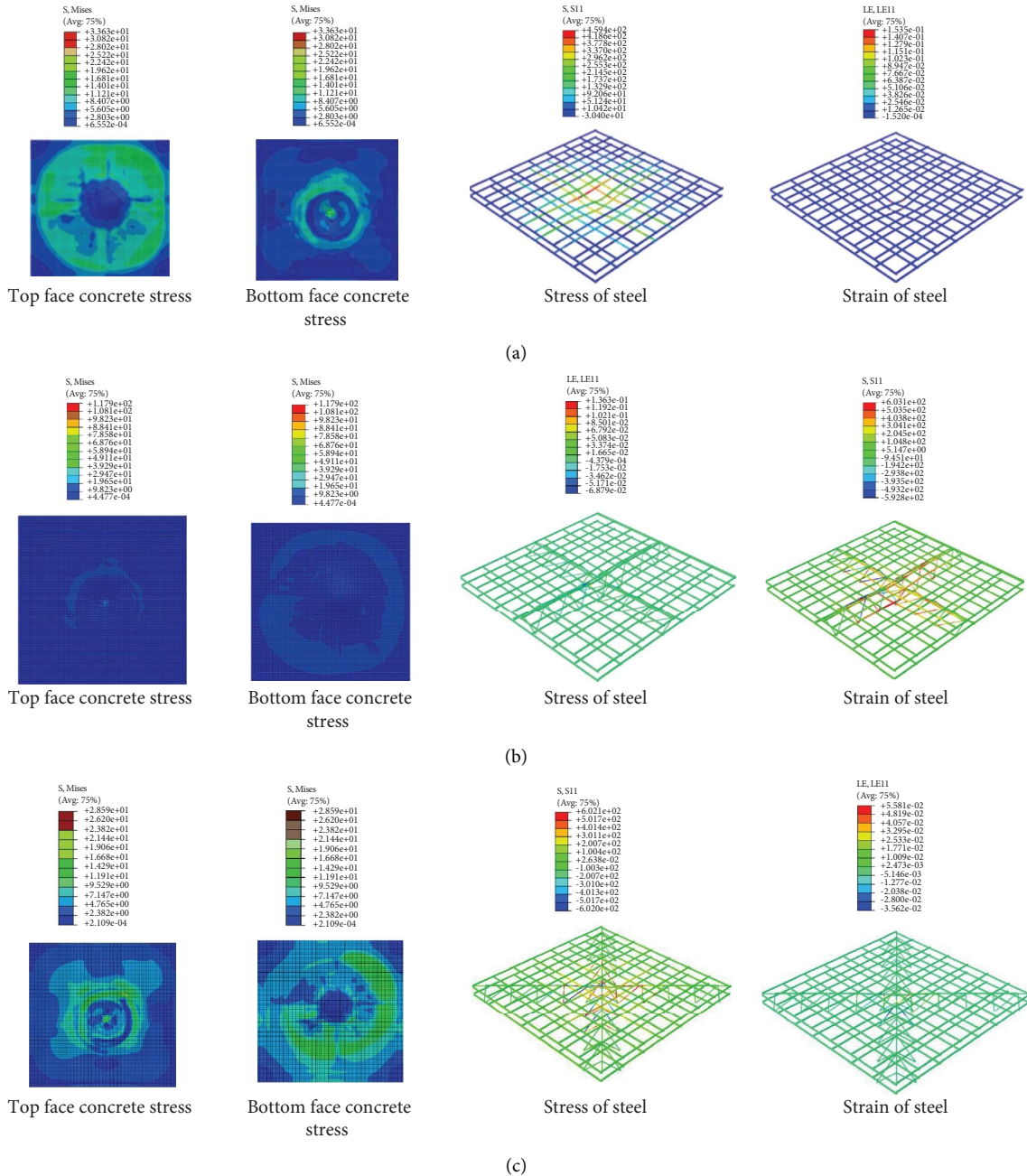
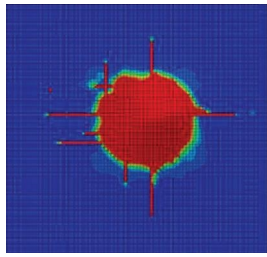
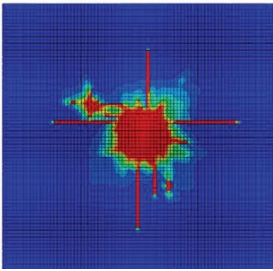
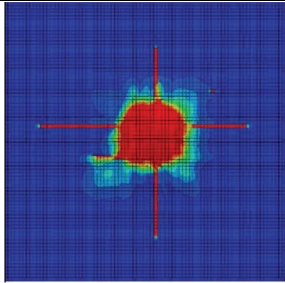


FIGURE 12: Graphical representation and numerical analysis of study samples. (a) Control sample (C $\phi 6$). (b) Sample with fabricated trussed bar shear reinforcement in the diagonal layout (TB $\phi 3$ Orth). (c) Sample with fabricated trussed bar shear reinforcement in the diagonal layout (TB $\phi 3$ Dia).

TABLE 9: Failure modes of parametric study samples.

Sample	Bottom face slab failure	Mode of damage
Ref C ϕ 6*		(i) Concrete scabbing (310 mm width) (ii) Flexural bond breakage (iii) Nonuniform diagonal fracturing
TB ϕ 3Orth		(i) Concrete scabbing at a width of 210 mm (ii) Failure of flexural bond (iii) Diagonal fractures exhibiting irregular patterns
TB ϕ 3Diag		(i) Scabbing in concrete (width: 230 mm) (ii) Failure in flexural bond (iii) Diagonal fractures with irregular patterns

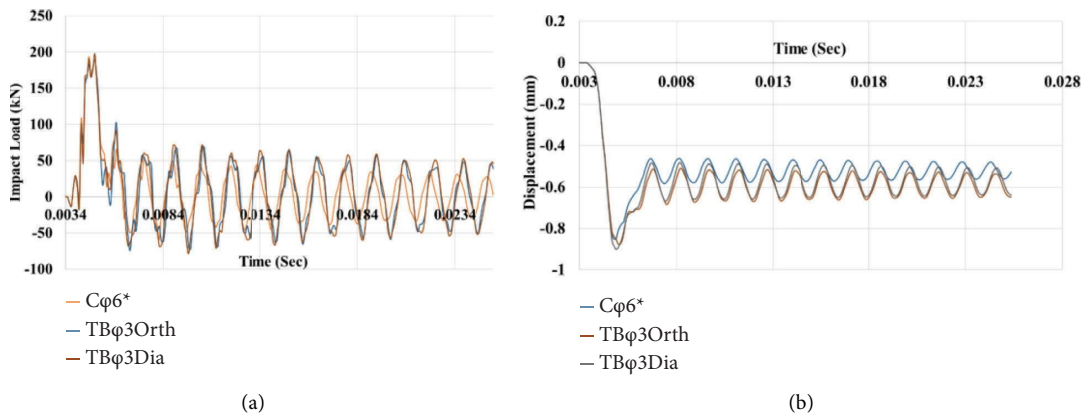


FIGURE 13: Impact load and displacement-time history of the study samples. (a) Impact load-time history of the samples at first drop. (b) Displacement-time history of the study samples at 20 mm from the center of the bottom face.

Altering the configuration of shear reinforcement in truss bars, shifting from orthogonal to diagonal, results in a reduction in the dissipated energy (DDE) from 55.2723 Joules for the orthogonal configuration (denoted as TB ϕ 3Orth*) to 40.8717 Joules for the diagonal configuration (referred to as TB ϕ 3Diag), representing a decrease of 26.05%, as elaborated in Table 10.

The diagonal arrangement of engineered truss bars, employed in reinforcing systems for slabs, manifests a pronounced impact on failure modalities [88]. Diagonally oriented reinforcement configurations [42, 61] have showcased remarkable efficacy in curtailing the extent of damage, encompassing phenomena such as concrete scabbing, spalling, and cracking within

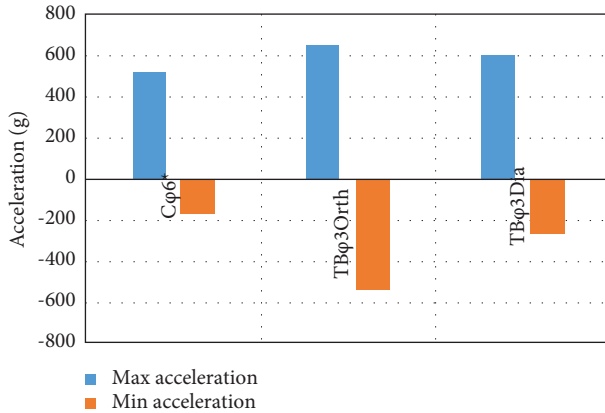


FIGURE 14: Maximum acceleration under the drop position at the first drop.

slabs. Notably, the slabs reinforced with diagonally oriented bars exhibit the least width and frequency of cracks.

5.2. Acceleration. In this study [41, 42, 48, 89], the evaluation predominantly relied on numerical estimations of acceleration, contrasting results primarily at the initial impact. The culmination of acceleration during impact reveals the inertia influence of the slab, intimately linked with its rigidity. The research underscores the significant impact of integrating shear reinforcement on the maximal vertical acceleration of the slab. Notably, slabs with denser reinforcement exhibit heightened accelerations compared to those with lighter reinforcement [90]. Figure 14 depicts the peak accelerations of 520.945 g (Cφ6), 649.565 g (TBφ3Orth), and 604.0968 g (TBφ3Dia) directly beneath the hammer, reflecting an increment of 24.701% and 15.972% relative to the control sample, respectively. The presence of steel beneath the impact zone notably influences the maximum acceleration.

Furthermore, transitioning from the orthogonal (TBφ3Orth) to diagonal (TBφ3Dia) configuration of truss bars induces a significant acceleration effect, resulting in a reduction of approximately 7.00% compared to the orthogonal arrangement. The utilization of diagonal layouts in previous reinforcement systems [42, 61, 91] has exhibited a marked elevation in acceleration metrics for RC slabs in comparison with configurations with strips arranged orthogonally or unidirectionally. This particular reinforcement design has proven more efficacious in bolstering the impact resilience of RC slabs.

5.3. Displacement and Stress. Table 10 presents a concise overview detailing the stress exerted on concrete and the subsequent displacement observed during both the initial descent and ultimate failure of the specimens under examination. Notably, when subjected to impacts at their upper and lower surfaces, both the standard sample and those augmented with custom truss bars exhibited discernible variations. Implementation of fabricated truss bars, whether in orthogonal or diagonal configurations, yielded

a noteworthy reduction in concrete stress at the upper surface by 8.372% and 9.805%, respectively, compared to the unaltered sample. Conversely, there was an elevation in concrete stress at the lower surface by 12.034% and 9.879% for orthogonal and diagonal layouts, respectively, in contrast to the control sample. The transition from the orthogonal (TBφ3Orth) to diagonal (TBφ3Dia) arrangement of the truss bars precipitated a modest decrease in concrete stress at both upper and lower surfaces during the initial descent, registering reductions of 1.5637% and 1.9231%, respectively. Notably, the stress endured by the concrete core of the standard sample and the modified specimen with truss bars amounted to 26.12 MPa and 18 MPa, respectively, following 124 successive impacts culminating in structural collapse. Furthermore, upon reaching the point of complete failure after 124 iterations, the stress experienced by the concrete at the central region of the upper surface was measured at 18 MPa for TBφ3Orth, while for TBφ3Dia, it escalated to 19.286 MPa, as illustrated in Figure 12.

Table 11 reveals the conspicuous declines in the strain exhibited by the upper and lower steel components positioned 200 mm away from the point of impact, suggesting that the inclusion of truss bars as shear reinforcement effectively promoted an equitable dispersion of stress and consequentially mitigated strain levels in the primary steel elements.

In terms of displacement, when situated 2 cm away from the central point of the bottom face, the standard control sample (Cφ6*) and specimens incorporating fabricated truss bars manifested displacements measuring 0.82087 mm and 0.87561 mm (TBφ3Orth), alongside 0.90107 mm (TBφ3Dia), respectively, during the initial descent. The introduction of fabricated truss bars resulted in displacement increments of 6.669% and 9.770% for both orthogonal and diagonal configurations compared to the baseline sample. Upon reaching complete failure subsequent to 124 drops, the displacement directly beneath the impactor for the control sample and those specimens featuring fabricated truss bars amounted to 26.50 mm, 9.1 mm (TBφ3Orth), and 18.787 mm (TBφ3Dia), respectively. Transitioning from an orthogonal to a diagonal arrangement of truss bars amplified the displacement at full failure by 106.4505% relative to TBφ3Orth, as depicted in Figure 13.

Ultimately, the residual displacement measured at a distance of 20 cm from the slab's center amounted to 0.522167342 mm for the Cφ6* configuration and 0.5944608 mm for TBφ3Orth, marking a 13.876% escalation relative to the baseline sample. The introduction of diagonal truss bar alignment, denoted as TBφ3Dia, yielded a reduction in residual displacement by -3.1525% compared to the orthogonal truss bar configuration (TBφ3Orth), as visually depicted in Figure 13(b).

The discoveries herein corroborate established methodologies for enhancing structural integrity, as cited, which effectively mitigate the deleterious effects of impact loading on RC slabs. This serves to mitigate fractures and underscores the efficacy of the strengthening technique in absorbing energy. Previous methodologies employing diagonal configurations in slab reinforcement have

TABLE 10: Results of parametric study samples.

Sample	Initial drop acceleration (g) at 20 cm from the center of the slab		Impact load (kN) at initial drop		Initial concrete stress (MPa) in the drop impact zone		Initial drop displacement (mm) measured 20 mm from the bottom face center		Initial drop-induced residual displacement (mm) at a 20 mm offset from the center of the slab's bottom face		Displacement (mm) at total failure beyond drop initiation position		DDE ⁺ (J) upon reaching total failure	
	Max	Min	Top face	Bottom face	Top face	Bottom face	Top face	Bottom face	Top face	Bottom face	Top face	Bottom face	Top face	Bottom face
C ϕ 6*	88.75617	-80.0309	195.54	19.03	102.6	19.03	0.82087	0.82087	0.5220267	0.5220267	26.501	26.501	77.205	77.205
TB ϕ 3Orth	88.646	-78.902	192.704	21.32	94.01	21.32	0.87561	0.87561	0.5944608	0.5944608	9.1	9.1	55.2723	55.2723
TB ϕ 3Dia	88.2752	-78.9325	204.619	20.91	92.54	20.91	0.90107	0.90107	0.5757206	0.5757206	18.787	18.787	40.8717	40.8717

*DDE: damage dissipation energy.

TABLE 11: Reduction in top and bottom steel strain at strain gauge locations upon complete failure.

Sample	Strain ($\mu\epsilon$)	
	Top steel	Bottom steel
C ϕ 6*	75.04	222.86
TB ϕ 3Orth	91.09	32.41
TB ϕ 3Dia	25.43	140.57

significantly influenced stress distribution, thereby attenuating the patterns of failure severity. Diagonal reinforcement arrangements facilitate the uniform propagation of stress waves, thereby subjecting the concrete to considerable dynamic loading during impulsive impacts. Consequently, the susceptibility to damage is diminished compared to control slabs and those employing conventional orientations [38, 39, 65].

The implementation of diagonal configurations in slab reinforcement systems has yielded notable effects on both vertical displacement and stress distribution. Strengthening methodologies [38], particularly when deployed diagonally in two orthogonal directions, have exhibited substantial reductions in the maximum displacement values induced by impacts. Furthermore, this specific reinforcement scheme has effectively curtailed both the width and quantity of cracks observed in the slabs.

The deployment of diagonal shear reinforcement orientation configurations [91] has facilitated a more uniform propagation of stress waves throughout the steel reinforcement network. Such configuration exposes the concrete to heightened dynamic loading forces during impulsive impacts, thereby permitting the concrete to manifest its optimal strength. As a result, slabs reinforced with a diagonal orientation demonstrate diminished structural deterioration in contrast to both the standard slab and slabs featuring conventional orientations. The efficacy of the diagonal pattern in bolstering the structural integrity and resilience of RC slabs under dynamic loading conditions is underscored by its proficiency in mitigating damage.

6. Conclusions

The principal aim of this investigation is to scrutinize and quantify the impact of a reinforcement technique on the low-velocity capabilities of RC slabs, incorporating shear reinforcement provided by fabricated truss bars. In order to maintain consistent input energy during impact loading, a 40 kg hammer was systematically released from a height of 450 mm in a succession of trials carried out within the scope of the study. Numerous measurements of acceleration, displacement, and strain were meticulously recorded to assess both the efficacy of the reinforcement procedure and the response of the slabs to impact [74, 92–96].

The RC slabs with shear reinforcement from produced truss bars underwent both the physical inspection and incremental dynamic analysis using the Abaqus software. The accuracy of the model was checked by simulating the impact behavior using a finite element model and comparing the numerical findings to experimental data. A comprehensive

analysis was conducted to ascertain the efficacy of employing truss bars as a means of augmenting the structural integrity of slabs against impact loads. This investigative inquiry adopted a parametric approach, juxtaposing various methods to discern the most potent solution. The investigation included a wide range of scenarios.

Based on the investigation conducted, a potential solution to the complexities entailed by antiquated and contemporary methods of fortifying RC slabs lies in the utilization of fabricated truss bar reinforcement. This alternative presents viable options for forthcoming strengthening systems aimed at enhancing the resilience of slabs against dynamic forces and potentially expediting the dissipation of impact loads. The primary conclusions drawn from the study are encapsulated as follows:

- (1) The integration of fabricated truss bars as shear reinforcement substantially enhanced the impact resistance of the slabs. Employing fabricated truss bars for shear reinforcement led to significant improvements in strength, rigidity, and ductility in contrast to specimens without such reinforcement. Notably, these enhancements were most evident when the fabricated truss bars were strategically placed in both orthogonal and diagonal configurations.
- (2) During impact loads, concrete crushing is the predominant failure mechanism. Implementing trussed bars as shear reinforcement, with a 3 mm diameter arranged orthogonally and diagonally, notably enhances slab resistance to damage. This reinforcement strategy results in a substantial reduction of 28.41% and 47.06% in DDE, respectively.
- (3) Fabricated trussed bars arranged orthogonally outperform those placed diagonally in terms of displacement and damage prevention, particularly with regard to perforation and splitting.
- (4) The integration of fabricated trussed bars as shear reinforcement significantly enhances the stiffness and toughness of RC slabs. Orthogonally arranged truss bars show a remarkable 24.701% increase, while diagonally placed bars exhibit a notable 15.972% enhancement compared to the control sample. Diagonally oriented truss bars notably bolster the impact resistance of RC slabs.
- (5) The orthogonal arrangement of fabricated truss bars for shear reinforcement significantly affects the performance of RC slabs under sudden dynamic impact loads. This configuration demonstrates reduced failure modes and increased maximum acceleration values, showing a notable improvement of about 7% compared to the diagonal layout.
- (6) The study shows that utilizing fabricated trussed bar shear reinforcement significantly improves the load capacity and impact resistance of slabs. This innovative reinforcement system, designed with vertically inclined links to enhance shear resistance, holds promise for enhancing overall structural

ductility. Incorporating this method substantially boosts both load capacity and impact ductility of slabs, with displacement increasing by 6.669% and 9.770% in orthogonal and diagonal layouts compared to the control sample.

- (7) In contrast to conventional laboratory experimentation, the utilization of finite element analysis via the Abaqus tool serves to authenticate test outcomes, thereby enhancing temporal efficiency while furnishing researchers with indispensable insights into structural reactions to impact loads.

Symbols

ρ :	Flexural tension reinforcement
ρ' :	Compression reinforcement
g :	Gravity acceleration
$\mu\epsilon$:	Microstrain
N :	Number of drops
m :	Mass
h :	Drop height
ν :	Poisson's ratio
E :	Elastic modulus of material
σ_{b0}/σ_{c0} :	Stress ratio (Abaqus User Guide, 2020)
K_c :	Shape factor
Ψ :	Dilation angle
μ :	Viscosity parameter
$v_{(\text{free-fall})}$:	Velocity of free fall
$t_{(\text{free-fall})}$:	Time of free fall
ϕ :	Bar diameter
Orth:	Orthogonal
Diag:	Diagonal
TB:	Truss bars
A_{st} :	Area of the shear reinforcement in the form of truss bars with two legs linked together
b :	Uniform spacing between the shear reinforcement
s :	Distance between vertical or inclined bars
ϕ_1 and ϕ_2 :	Angles between the front of the truss bars reinforcement and the vertical link and positioned between the truss bars reinforcement and the axis that is perpendicular to the shear force
DDE:	Damage dissipation energy
*	Reference sample.

Data Availability

All information provided in the conclusion is presented in the full document.

Ethical Approval

This work did not report on or involve the use of any animal or human data or tissue.

Consent

All participants gave their consent for their data to be published in the journal article.

Conflicts of Interest

The authors declare that there are no conflicts of interest.

Authors' Contributions

Rayeh Nasr Al-Dala'ien conceived the study; Rayeh Nasr Al-Dala'ien and S. M. Anas curated the data; Rayeh Nasr Al-Dala'ien, Abdel-Fattah Jamal Kodrg, and S. M. Anas contributed to the formal analysis; Rayeh Nasr Al-Dala'ien and S. M. Anas investigated the study; Rayeh Nasr Al-Dala'ien helped with methodology; Abdel-Fattah Jamal Kodrg helped with software; S. M. Anas supervised the study; Rayeh Nasr Al-Dala'ien and Abdel-Fattah Jamal Kodrg validated the study. Rayeh Nasr Al-Dala'ien wrote the original draft of the manuscript; and S. M. Anas reviewed and edited the manuscript.

References

- [1] S. M. Anas, R. N. Al-Dala'ien, R. Tahzeeb, M. Shariq, and M. Alam, "A concise overview of numerical simulation tools and techniques for anti-explosion response prediction of infrastructures and facilities," in *E3S Web of Conferences*, EDP Sciences, Les Ulis, Europe, 2023.
- [2] S. M. Anas, M. Alam, and M. Shariq, "Damage response of conventionally reinforced two-way spanning concrete slab under eccentric impacting drop weight loading," *Defence Technology*, vol. 19, pp. 12–34, 2023.
- [3] E. K. S. Al-Hachamee, "Effect of boundary conditions on impact stresses of beams," *Tikrit Journal of Engineering Sciences*, vol. 13, no. 3, pp. 78–102, 2006.
- [4] S. D. Adhikary, B. Li, and K. Fujikake, "Dynamic behavior of reinforced concrete beams under varying rates of concentrated loading," *International Journal of Impact Engineering*, vol. 47, pp. 24–38, 2012.
- [5] J. Özbolt and A. Sharma, "Numerical simulation of reinforced concrete beams with different shear reinforcements under dynamic impact loads," *International Journal of Impact Engineering*, vol. 38, no. 12, pp. 940–950, 2011.
- [6] F. Stochino and G. Carta, "SDOF models for reinforced concrete beams under impulsive loads accounting for strain rate effects," *Nuclear Engineering and Design*, vol. 276, pp. 74–86, 2014.
- [7] T. M. Pham and H. Hao, "Influence of global stiffness and equivalent model on prediction of impact response of RC beams," *International Journal of Impact Engineering*, vol. 113, pp. 88–97, 2018.
- [8] S. A. Derseh, G. Urgessa, and T. A. Mohammed, "Finite element analysis of the response of conventional and special reinforcement detailed concrete beams subjected to impact loads," *Structures*, vol. 52, pp. 57–82, 2023.
- [9] Q. M. Shakir and H. K. Hannon, "New models for reinforced concrete precast hybrid deep beams under static loads with curved hybridization," in *Structures*, pp. 1007–1025, Elsevier, Amsterdam, The Netherlands, 2023.
- [10] Q. M. S. Al-Abbasi and H. K. Hannon, "Enhancing the structural performance of the reinforced precast concrete hybrid deep beams based on tied-arch action," *Journal of Building Pathology and Rehabilitation*, vol. 9, no. 1, p. 18, 2024.
- [11] Q. M. Shakir, H. K. Hannon, and E. Noroozinejad Farsangi, "Enhancing the performance of precast hybrid concrete deep beams using curved and arched designs: experimental investigations," *Structures*, vol. 58, Article ID 105371, 2023.

- [12] A. Remennikov and S. Kaewunruen, "Impact resistance of reinforced concrete columns: experimental studies and design considerations," 2006, <https://ro.uow.edu.au/engpapers/379>.
- [13] O. I. Abdelkarim and M. A. ElGawady, "Performance of hollow-core FRP-concrete-steel bridge columns subjected to vehicle collision," *Engineering Structures*, vol. 123, pp. 517–531, 2016.
- [14] T. V. Do, T. M. Pham, and H. Hao, "Numerical investigation of the behavior of precast concrete segmental columns subjected to vehicle collision," *Engineering Structures*, vol. 156, pp. 375–393, 2018.
- [15] S. Auyeung, A. Alipour, and D. Saini, "Performance-based design of bridge piers under vehicle collision," *Engineering Structures*, vol. 191, pp. 752–765, 2019.
- [16] Ö. Çalışkan, M. Aras, T. Yılmaz, Ö. Anıl, and R. T. Erdem, "Impact behavior of low strength concrete slab strengthened with fan type anchored carbon fiber-reinforced polymer strips," *Structural Concrete*, vol. 24, no. 1, pp. 1689–1711, 2023.
- [17] T. J. Vijay, M. M. Kumar, G. Sofia, and R. Abiraami, "Impact behaviour of reinforced concrete slabs embedded with inclined reinforcements," *Materials Today Proceedings*, 2020.
- [18] Y. Arsan, *Effects of Shear Reinforcement on the Impact Behavior of Reinforced concrete Slabs*, Izmir Institute of Technology, İzmir, Türkiye, 2014.
- [19] W. Chen, T. M. Pham, M. Elchalakani, H. Li, H. Hao, and L. Chen, "Experimental and numerical study of Basalt FRP strip strengthened RC slabs under impact loads," *International Journal of Structural Stability and Dynamics*, vol. 20, no. 06, p. 2040001, 2020.
- [20] T. H. Almusallam, A. A. Abadel, Y. A. Al-Salloum, N. A. Siddiqui, and H. Abbas, "Effectiveness of hybrid-fibers in improving the impact resistance of RC slabs," *International Journal of Impact Engineering*, vol. 81, pp. 61–73, 2015.
- [21] J. Y. Lee, T. F. Yuan, D. Y. Yoo, and Y. S. Yoon, "Benefits of using fiber on impact resistance of FRC slabs," *MATEC Web of Conferences*, vol. 138, p. 03009, 2017.
- [22] K. Kamran, M. Khan, and M. Iqbal, "An experimental investigation of plain, reinforced, and prestressed concrete slabs subjected to non-deformable projectile impact," *Engineering Failure Analysis*, vol. 159, Article ID 108090, 2024.
- [23] V. Kumar, M. A. Iqbal, and A. K. Mittal, "Impact resistance of prestressed and reinforced concrete slabs under falling weight indenter," in *Procedia Structural Integrity*, pp. 95–100, Elsevier B.V, Amsterdam, The Netherlands, 2017.
- [24] D. G. Gaidhankar, M. O. Naqshbandi, and M. S. Kulkarni, "Impact strength of ferrocement panel under low velocity impact loading," *Regular issue*, vol. 10, no. 5, pp. 285–291, 2021.
- [25] V. Hugo Dalosto de Oliveira, H. Jorge Nery de Lima, and G. Sales Melo, "Punching shear resistance of flat slabs with different types of stirrup anchorages such as shear reinforcement," *Engineering Structures*, vol. 253, Article ID 113671, 2022.
- [26] G. S. Melo, M. P. Ferreira, H. J. Lima et al., "Effect of the shear reinforcement anchorage and detailing on the punching resistance of flat slabs," *International Concrete Abstracts Portal*, vol. 357.
- [27] T. S. Eom, J. W. Song, J. K. Song, G. S. Kang, J. K. Yoon, and S. M. Kang, "Punching-shear behavior of slabs with bar truss shear reinforcement on rectangular columns," *Engineering Structures*, vol. 134, pp. 390–399, 2017.
- [28] Aci 318, "318M–19: building code requirements for reinforced concrete and commentary," p. 261, 2019, <https://dogoharani.com/wp-content/uploads/2021/03/ACI-318M-19-Metric.pdf>.
- [29] M. P. Ferreira, M. J. M. Pereira Filho, M. V. P. Freitas, A. F. Lima Neto, and G. S. S. A. Melo, "Experimental resistance of slab-column connections with prefabricated truss bars as punching shear reinforcement," *Engineering Structures*, vol. 233, Article ID 111903, 2021.
- [30] R. S. Pinto, V. C. Sousa, L. S. Tapajós, M. D. P. Ferreira, and A. F. Lima Neto, "Influence of the supplementary reinforcement on the shear strength of beams with prefabricated truss stirrups," *Revista IBRACON de Estruturas e Materiais*, vol. 15, no. 1, 2022.
- [31] A. S. G. Qanber, M. H. Yas, and M. M. Kadhum, "Numerical and experimental behavior analysis of slabs strengthened using steel plates and slurry-infiltrated Mat concrete (SIMCON) laminates," *Infrastructure*, vol. 8, no. 5, p. 85, 2023.
- [32] M. H. Yas, M. M. Kadhum, and W. G. B. Al-Dhufairi, "Development of an engineered slurry-infiltrated fibrous concrete: experimental and modelling approaches," *Infrastructure*, vol. 8, no. 2, p. 19, 2023.
- [33] R. Z. Al-Rousan, "Failure analysis of polypropylene fiber reinforced concrete two-way slabs subjected to static and impact load induced by free falling mass," *Latin American Journal of Solids and Structures*, vol. 15, no. 1, 2018.
- [34] T. J. Vijay, K. Rajesh Kumar, R. Vandhiyan, K. Mahender, and K. Tharani, "Performance of geogrid reinforced concrete slabs under drop weight impact loading," in *IOP Conference Series: Materials Science and Engineering*, IOP Publishing Ltd, Bristol, UK, 2020.
- [35] B. Batarlar, M. Hering, F. Bracklow, T. Kühn, B. Beckmann, and M. Curbach, "Experimental investigation on reinforced concrete slabs strengthened with carbon textiles under repeated impact loads," *Structural Concrete*, vol. 22, no. 1, pp. 120–131, 2021.
- [36] S. M. Anas, M. Alam, and F. A. Uriyar, "Response of singly reinforced square concrete slab with varying standard concrete strength and slab thickness under concentric impact loading: a numerical study," *International Journal of Applied Systemic Studies*, vol. 1, no. 1, p. 1, 2023.
- [37] A. I. Said and E. M. Mouwainea, "Behaviours of reinforced concrete slabs under static loads and high-mass low velocity impact loads," *IOP Conference Series: Materials Science and Engineering*, vol. 1067, no. 1, Article ID 012036, 2021.
- [38] Y. Wang, J. Liu, Z. Xiao, F. Zhao, and Y. Cheng, "Experiment and simulation study on the dynamic response of RC slab under impact loading," *Shock and Vibration*, vol. 2021, Article ID 7127793, 15 pages, 2021.
- [39] E. M. Mouwainea and A. M. I. Said, "Numerical modeling of reinforced concrete slabs under impact loading," in *Key Engineering Materials*, pp. 99–108, Trans Tech Publications Ltd, Stafa-Zurich, Switzerland, 2020.
- [40] M. Hering, T. Kühn, M. Curbach, and U. Häußler-Combe, "Reinforced concrete slabs under impact – scale effects," *Fib Symposium*, pp. 1–10, 2016.
- [41] H. Selim Şengel, H. Erol, T. Yılmaz, Ö. Anıl, H. Can Gürdal, and A. Muhammed Uludoğan, "Low-velocity impact behavior of two-way RC slab strengthening with carbon TRM strips," *Structures*, vol. 44, pp. 1695–1714, 2022.
- [42] T. Yılmaz, N. Kırac, Ö. Anıl, R. T. Erdem, and C. Sezer, "Low-velocity impact behaviour of two way RC slab strengthening with CFRP strips," *Construction and Building Materials*, vol. 186, pp. 1046–1063, 2018.
- [43] A. I. Said and E. M. Mouwainea, "Experimental study of reinforced concrete slabs strengthened by CFRP subjected to impact loads," in *IOP Conference Series: Earth and Environmental Science*, IOP Publishing Ltd, Bristol, UK, 2021.

- [44] Z. Huang, Y. Zhao, J. Zhang, and Y. Wu, "Punching shear behaviour of concrete slabs reinforced with CFRP grids," *Structures*, vol. 26, pp. 617–625, 2020.
- [45] H. Othman and H. Marzouk, "Impact resistance of UHPFRC plates," *AFGC-ACI-fib-RILEM Int. Symposium on Ultra-High Performance Fibre-Reinforced Concrete*, vol. 1, pp. 403–410, 2017.
- [46] S. M. Anas, M. Alam, H. F. Isleem, H. M. Najm, and M. M. S. Sabri, "Ultra high performance concrete and C-FRP tension Re-bars: a unique combinations of materials for slabs subjected to low-velocity drop impact loading," *Front Mater*, vol. 9, 2022.
- [47] S. M. Anas, M. Alam, and M. Shariq, "Behavior of two-way RC slab with different reinforcement orientation layouts of tension steel under drop load impact," *Materials Today Proceedings*, vol. 87, no. 1, 2022.
- [48] M. Zineddin and T. Krauthammer, "Dynamic response and behavior of reinforced concrete slabs under impact loading," *International Journal of Impact Engineering*, vol. 34, no. 9, pp. 1517–1534, 2007.
- [49] T. D. Hrynyk and F. J. Vecchio, "Behavior of steel fiber-reinforced concrete slabs under impact load," *ACI Structural Journal*, vol. 111, no. 5, pp. 1213–1224, 2014.
- [50] T. Yılmaz, N. Kırac, Ö. Anil, R. T. Erdem, and G. Kaçaran, "Experimental investigation of impact behaviour of RC slab with different reinforcement ratios," *KSCE Journal of Civil Engineering*, vol. 24, no. 1, pp. 241–254, 2020.
- [51] S. D. Adhikary, B. Li, and K. Fujikake, "State-of-the-art review on low-velocity impact response of reinforced concrete beams," *Magazine of Concrete Research*, vol. 68, no. 14, pp. 701–723, 2016.
- [52] H. Othman and H. Marzouk, "An experimental investigation on the effect of steel reinforcement on impact response of reinforced concrete plates," *International Journal of Impact Engineering*, vol. 88, pp. 12–21, 2016.
- [53] R. Tuğrul Erdem, "Dynamic responses of reinforced concrete slabs under sudden impact loading," *Revista de la Construcción*, vol. 20, no. 2, pp. 346–358, 2021.
- [54] M. Zineddin, "Simulation of reinforced concrete slab behavior under impact loading," in *Proceedings of the AEI 2008 Conference- AEI 2008: Building Integration Solutions*, September 2008.
- [55] R. Abdullah and S. Niza Mokhtar, "Computational analysis of reinforced concrete slabs subjected to impact loads," 2012, <https://www.researchgate.net/publication/276928201>.
- [56] S. M. Anas and M. Alam, "Role of shear reinforcements on the punching shear resistance of two-way RC slab subjected to impact loading," *Materials Today: Proceedings*, vol. 87, pp. 43–54, 2023.
- [57] F. Tahmasebinia and A. Remennikov, "Simulation of the reinforced concrete slabs under impact loading simulation of the reinforced concrete slabs under impact loading," *Australasian Structural Engineering Conference (ASEC)*, vol. 10, 2008, <http://ro.uow.edu.au/engpapers/3224>.
- [58] R. N. Al-Dala'ien, A. Syamsir, M. S. Abu Bakar, F. Usman, and M. J. Abdullah, "Effect of the stirrup shear reinforcement on the dynamic behavior and failure modes of two-way reinforced concrete slab subjected to the low-velocity impact loading," *Arabian Journal for Science and Engineering*, vol. 49, 2023.
- [59] F. Tahmasebinia, "Simulation of the reinforced concrete slabs under dynamic loading," *IABSE Conference, Helsinki 2008: Information and Communication Technology (ICT) for Bridges, Buildings and Construction Practice*, vol. 94, no. 13, pp. 25–31, 2008.
- [60] F. Tahmasebinia, "Numerical modelling of reinforced concrete slabs subject to impact loading," *University Of Wollongong Thesis Collection*, vol. 215, 2008.
- [61] Y. T. Obaidat, S. Heyden, and O. Dahlblom, "The effect of CFRP and CFRP/concrete interface models when modelling retrofitted RC beams with FEM," *Composite Structures*, vol. 92, no. 6, pp. 1391–1398, 2010.
- [62] K. Sun, Y. Wu, S. Li, Y. Feng, and L. Feng, "Study on dynamic impact mechanical properties of UHPC with high-content and directional reinforced steel fiber," *Applied Sciences*, vol. 13, no. 6, p. 3753, 2023.
- [63] E. Tekleab and T. Wondimu, "Behavior of steel-fiber-reinforced concrete (SFRC) slab-on-grade under impact loading," *Advances in Civil Engineering*, vol. 2022, Article ID 6232757, 18 pages, 2022.
- [64] T. Hrynyk and F. J. Vecchio, "Modeling of reinforced and fiber-reinforced concrete slabs under impact loads," 2017, <https://www.researchgate.net/publication/320716445>.
- [65] T. D. Hrynyk and F. J. Vecchio, "Modeling of reinforced concrete slabs under high-mass low-velocity impact," *Response of Structures Under Extreme Loading (PROTECT 2015)*, 2015.
- [66] C. Zhang, G. Gholipour, and A. A. Mousavi, "State-of-the-Art review on responses of RC structures subjected to lateral impact loads," *Archives of Computational Methods in Engineering*, vol. 28, no. 4, pp. 2477–2507, 2021.
- [67] R. N. Al-Dala'ien, A. Syamsir, A.-F. J. Kodrg, F. Usman, and M. J. Abdullah, "The effect of continuous rectangular spiral shear reinforcement on the dynamic behavior of RC solid slab subjected to low-velocity impact loading," *Results in Engineering*, vol. 21, Article ID 101942, 2024.
- [68] M. Azimi, A. Bagherpourhamedani, M. M. Tahir, A. R. Bin Mohd Sam, and C. K. Ma, "Evaluation of new spiral shear reinforcement pattern for reinforced concrete joints subjected to cyclic loading," *Advances in Structural Engineering*, vol. 19, no. 5, pp. 730–745, 2016.
- [69] W. De Corte and V. Boel, "Effectiveness of spirally shaped stirrups in reinforced concrete beams," *Engineering Structures*, vol. 52, pp. 667–675, 2013.
- [70] A. A. Elansary, Y. Y. Elnazlawy, and H. A. Abdalla, "Shear behaviour of concrete wide beams with spiral lateral reinforcement," *Australian Journal of Civil Engineering*, vol. 20, no. 1, pp. 174–194, 2022.
- [71] C. G. Karayannis and C. E. Chalioris, "Shear tests of reinforced concrete beams with continuous rectangular spiral reinforcement," *Construction and Building Materials*, vol. 46, pp. 86–97, 2013.
- [72] A. Cemalettin Dönmez and A. Mert Yücel Yardimci, "Effects of shear reinforcement on the impact behavior of reinforced concrete slabs," *ACI Structural Journal*, vol. 106, no. 1, pp. 78–86, 2014.
- [73] ASTM, "ASTM E8/E8M standard test methods for tension testing of metallic materials 1," *Annual Book of ASTM Standards*, vol. 4, pp. 1–27, 2010.
- [74] F. Monney, Q. Yu, M. Fernández Ruiz, and A. Muttoni, "Anchorage of shear reinforcement in beams and slabs," *Engineering Structures*, vol. 265, Article ID 114340, 2022.
- [75] E. Rizk and H. Marzouk, "Minimum shear reinforcement for thick plates and two-way slabs," *Engineering Structures*, vol. 46, pp. 1–13, 2013.
- [76] M. P. Ferreira, Federal University of Para Brazil, R. N. M. Barros, M. J. M. Pereira Filho, L. S. Tapajós, and F. S. Quaresma, "One-way shear resistance of RC members with unconnected stirrups," *Latin American Journal of Solids and Structures*, vol. 13, no. 15, pp. 2970–2990, 2016.

- [77] ACI PRC, *Guide to Shear Reinforcement for Slabs*, American Concrete Institute, Farmington Hills, MI, USA, 2008.
- [78] B S I, *BS EN 12390-3: 2019: Testing Hardened Concrete. Part 3: Compressive Strength of Test Specimens*, BSI British Standards Institution, London, UK, 2022.
- [79] En 1992-1-1, "Eurocode 2: design of concrete structures- Part 1-1: general rules and rules for buildings," 2004, <https://www.phd.eng.br/wp-content/uploads/2015/12/en.1992.1.1.2004.pdf>.
- [80] J. Tonello, "Généralités et approche de modeles simples," *Stage Paravalanches*, ENPC, Paris, France, 1988.
- [81] A. S. U. Manual, "Abaqus 6.11," 2012, <http://130.149>.
- [82] F. Lin, Y. Dong, X. Kuang, and L. Lu, "Strain rate behavior in tension of reinforcing steels HPB235, HRB335, HRB400, and HRB500," *Materials*, vol. 9, no. 12, p. 1013, 2016.
- [83] T. Yilmaz, Ö. Anil, and R. T. Erdem, "Experimental and numerical investigation of impact behavior of RC slab with different opening size and layout," in *Structures*, pp. 818–832, Elsevier, Amsterdam, The Netherlands, 2022.
- [84] Ö. Anil, E. Kantar, and M. C. Yilmaz, "Low velocity impact behavior of RC slabs with different support types," *Construction and Building Materials*, vol. 93, pp. 1078–1088, 2015.
- [85] M. J. Abdullah, "The strength and thermal properties of concrete containing water absorptive aggregate from well-graded bottom ash (BA) as partial sand replacement," *Construction and Building Materials*, vol. 339, Article ID 127658, 2022.
- [86] M. Hafezolghorani, F. Hejazi, R. Vaghei, M. S. Bin Jaafar, and K. Karimzade, "Simplified damage plasticity model for concrete," in *Structural Engineering International, Int. Assoc. For Bridge and Structural Eng*, pp. 68–78, Eth-Honggerberg, Zürich, Switzerland, 2017.
- [87] A. Goswami, S. D. Adhikary, and B. Li, "Predicting the punching shear failure of concrete slabs under low velocity impact loading," *Engineering Structures*, vol. 184, pp. 37–51, 2019.
- [88] S. M. Anas, M. Alam, and M. Shariq, "Behavior of two-way RC slab with different reinforcement orientation layouts of tension steel under drop load impact," *Materials Today: Proceedings*, vol. 87, pp. 30–42, 2023.
- [89] S. M. Anas, M. Alam, and R. Tahzeeb, "Impact response prediction of square RC slab of normal strength concrete strengthened with (1) laminates of (i) mild-steel and (ii) C-FRP, and (2) strips of C-FRP under falling-weight load," *Materials Today: Proceedings*, vol. 87, pp. 9–19, 2023.
- [90] M. Zineddin and T. Krauthammer, "Dynamic response and behavior of reinforced concrete slabs under impact loading," *International Journal of Impact Engineering*, vol. 34, no. 9, pp. 1517–1534, 2007.
- [91] M. Loganaganandan, G. Murali, M. P. Salaimanimagudam, M. K. Haridharan, and K. Karthikeyan, "Experimental study on GFRP strips strengthened new two stage concrete slabs under falling mass collisions," *KSCE Journal of Civil Engineering*, vol. 25, no. 1, pp. 235–244, 2021.
- [92] Y. Xiao, B. Li, and K. Fujikake, "Behavior of reinforced concrete slabs under low-velocity impact," *ACI Structural Journal*, vol. 114, no. 3, pp. 643–658, 2017.
- [93] S. D. Adhikary, B. Li, and K. Fujikake, "Low velocity impact response of reinforced concrete beams: experimental and numerical investigation," *International Journal of Protective Structures*, vol. 6, no. 1, pp. 81–111, 2015.
- [94] R. N. Al-Dala'ien, A. Syamsir, F. Usman, and M. J. Abdullah, "The effect of the W-shape stirrups shear reinforcement on the dynamic behavior of RC flat solid slab subjected to the low-velocity impact loading," *Results in Engineering*, vol. 19, Article ID 101353, 2023.
- [95] D. F. D. Souza, J. H. C. Abrantes, L. S. Tapajós, M. D. P. Ferreira, and A. F. Lima Neto, "Shear in reinforced concrete beams with continuous internal transverse reinforcement," *Revista IBRACON de Estruturas e Materiais*, vol. 16, no. 1, 2023.
- [96] M. Husem and S. I. Cosgun, "Behavior of reinforced concrete plates under impact loading: different support conditions and sizes," *Computers and Concrete*, vol. 18, no. 3, pp. 389–404, 2016.